Materials Science in Semiconductor Processing 71 (2017) 427–432

Contents lists available at ScienceDirect

Materials Science in Semiconductor Processing

journal homepage: www.elsevier.com/locate/mssp

# High performance $TiO_2$ nanotubes antireflection coating

Daniel Fabián Rodríguez[a], Patricia María Perillo[a,*], Marcela Patricia Barrera[b,c]

[a] Departamento de Micro y Nanotecnología, Centro Atómico Constituyentes, Comisión Nacional de Energía Atómica, Av. Gral. Paz 1499 (1650) Bs As., Argentina
[b] Departamento de Energía Solar, Centro Atómico Constituyentes, Comisión Nacional de Energía Atómica, Av. Gral. Paz 1499 (1650) Bs As., Argentina
[c] Consejo Nacional de Investigaciones Científicas y Técnicas, Av. Rivadavia 1917 (1033) Bs As., Argentina

ARTICLE INFO

*Keywords:*
$TiO_2$
Antireflection
Spectroscopic ellipsometry
Nanotubes

ABSTRACT

The present study analyzes the use of $TiO_2$ layer as antireflection coating. $TiO_2$ thin films were prepared on silicon substrate by electrochemical anodization process with thicknesses of 130 and 170 nm. The films exhibit a uniform nanotubular structure. The ellipsometry measurement data were analyzed using a multi-layer model, the bottom layer is a dense layer of $TiO_2$ and the top layers are porous; they are formed by a mixture of $TiO_2$ and void. The values of refractive index are obtained by the Bruggeman effective medium approximation. The refractive indexes of the bottom and top $TiO_2$ sublayers were about 2.3 and 1.6, respectively. The lower values of reflectance are obtained with the thinnest film. For these samples the reflectance decreases about 90% compared to silicon and in some cases the reflectivity is less than 5%. The thickness influences of $TiO_2$ thin films and their synthesis parameters on the optical constants are discussed.

## 1. Introduction

$TiO_2$ nanostructured has been found to possess a variety of highly useful applications, including their use in gas sensors [1–3], solar cells [4,5], photocatalysis [6,7], UV photodetectors [8,9], supercapacitors [10,11] and so on. It has been widely used in optoelectronic devices due to its excellent electrical and optical properties. Particularly, one way to increase the efficiency of solar cells is to implement antireflective coatings (ARC). Considering silicon solar cells, this material reflects from 30% in the infrared light to more than 60% in the ultraviolet light. For this reason is necessary to minimize the reflected light at the front surface and thus increase the absorbed energy. Suitable materials as antireflective coatings are $TiO_2$, $SiO_2$, $Al_2O_3$ and ZnS [12–14].

Antireflection coatings can be based on homogeneous layers or on inhomogeneous coatings [15]. An example of the homogeneous case is thin dielectric multilayers, which consists in stack the layers so that the index of refraction is decreasing from the substrate to the air to reduce the apparent abruptness of the interface. An example of the inhomogeneous case could be ARC focusing on the material and its topography, such as porous or textured surface of the substrate or the coating [16]. The work of Xi et al. [17] presents nanorods grown by oblique-angle deposition using electron beam evaporation. Other research group works in ZnO nanotubes, fabricated by hydrothermal growth on triple junction solar cell devices [18]. In the homogenous case, as in the inhomogeneous case, graduated effective index coatings are obtained.

On the other hand, the manufacturing of solar cells with ARC requires compatibility between the manufacturing stages of the ARC and the manufacturing process of the device.

This work is focused on the study of antireflective films of $TiO_2$ nanotubes compatible with silicon solar cells. The films were prepared by anodic oxidation method, which offer good optical performance, excellent adherence and are compatible with the process of manufacturing solar cells at laboratory scale.

## 2. Materials and methods

### 2.1. Deposition of a Ti thin film on a Si substrate

Titanium (Ti) films were deposited by magnetron sputtering on p-type silicon (Si) (100) wafer at room temperature. Target of 99.9% Ti with 50 and 6 mm in diameter and thickness, respectively, was used as the material source. The chamber pressure was maintained at 0.4 Pa during the deposition process.

Sputtering was carried by pure argon with 8 $cm^3$/min volume flow rate. The distance between the target and the substrate was 14 cm and the sputtering power was 160 W using a DC power supply. Under these conditions, the deposition rate was 4.4 nm/min and 80 and 120 nm thick Ti films were obtained after 18 and 27 nm, respectively.

* Corresponding author.
*E-mail addresses:* daniel.cnea@gmail.com (D.F. Rodríguez), perillo@cnea.gov.ar (P.M. Perillo), barrera@tandar.cnea.gov.ar (M.P. Barrera).

http://dx.doi.org/10.1016/j.mssp.2017.08.037
Received 25 July 2017; Received in revised form 29 August 2017; Accepted 31 August 2017
1369-8001/ 

**Table 1**
Parameters for the anodization process of Ti thin films.

| Sample | Voltage | Time | Sample | Voltage | Time |
|---|---|---|---|---|---|
| T-1 | 20 V | 700 s | M-1 | 20 V | 1200 s |
| T-2 | 30 V | 600 s | M-2 | 30 V | 800 s |
| T-3 | 30 V | 500 s | M-3 | 30 V | 900 s |
| T-4 | 30 V | 400 s | M-4 | 30 V | 1000 s |
| T-5 | 40 V | 300 s | M-5 | 30 V | 1200 s |

### 2.2. Preparation of $TiO_2$ nanotubes

Highly ordered, vertically oriented $TiO_2$ nanotube-arrays were fabricated by potentiostatic anodization of titanium. The anodization was conducted in a two electrode electrochemical cell with a platinum foil as cathode and Si substrate with Ti as anode at a constant potential. The growth of the nanotube arrays has been obtained in a glycerol solution with 0.6 wt% $NH_4F$ at room temperature. Anodization was performed applying a potential ramp of 1 V/s until it reached the desired voltage using a Keithley 2612A system sourcemeter. The detailed procedure for the preparation of $TiO_2$ nanotubes is described in our previous works [19,20].

The samples are grouped into two series according to the thickness of the Ti film prior to electrochemical anodization. The set corresponding to 80 and 120 nm of thickness is indicated with the letter T and M, respectively. The parameters for the anodization of Ti films are shown in Table 1.

After the electrochemical treatment, the samples were immediately washed with deionized water and dried in nitrogen stream. Finally, in order to convert the amorphous $TiO_2$ structure into a crystalline one, samples were annealed at 350 °C for 2 h in air [21].

### 2.3. Film characterization

The structural analysis of the films was carried out using Grazing Incidence X-Ray Diffraction (GIXRD), with a PANalytical model Empyrean diffractometer equipped Cu Kα radiation (λ = 0,15418 nm) using a generator voltage of 40 kV and current of 40 mA, operating at θ = 2°.

Scanning electron microscope (SEM) Zeiss model Supra40 Gemini was employed for the morphological characterization of the $TiO_2$ samples.

Spectroscopic ellipsometer (SE) Horiba model AUTO-SE was used to examine the optical property in the wavelength range between 400 and 800 nm and at a constant angle of incidence of 69.95°.

The spectral hemispherical reflectivity was measured with a GMC UV–Vis 920 spectrophotometer with an integrating sphere at almost normal incidence.

## 3. Results and discussion

### 3.1. Structural and morphology of the films

Fig. 1 shows SEM images cross-sectional of $TiO_2$ films prepared by electrochemical anodization after annealing.

The films have (Fig. 1a–b) thicknesses about 130 and 170 corresponding to the sample of 80 and 120 of Ti film thickness respectively. In Image 1b it can be seen clearly two zones: a compact lower and a higher columnar. Fig. 2 shows the top-view images of the TiO2 sample M-1 at two magnifications,

The length expansion when the Ti is converted to $TiO_2$ is about 50%. The length expansion can be explained by the Pilling-Bedworth ratio (PBR). This factor represents the ratio of the volume per metal ion in the oxide to the volume per metal atom in the titanium. The PBR strongly depends on the applied anodization potential and the electrolyte used [22,23].

From the top view, the SEM image of all samples exhibits a uniform nanotubular structure. All the nanotubes have an inner diameter of ~ 20–40 nm. These results are consistent with the literature [24,25].

Fig. 3 shows the XRD patterns of the sample M-1 after annealed. The peaks are indexed as the anatase phase (01-086-1157) and rutile (00-034-0180). The ratio of the phases depends strongly on the heat treatment but also depends on the anodizing voltage. The samples crystallized into two phases with anatase dominant at lower temperature and then the more stable rutile appeared when the temperature was raised [21].

### 3.2. Reflectivity measurements

The reflectance of the $TiO_2$ films and silicon are shown in Fig. 4a–b. The lower values of reflectance are obtained with the thinnest film (T). For these samples the reflectance decreases about 90% compared to silicon. It can also be noted that in some cases the reflectivity is less than 5% (Fig. 4a). In contrast, for thicker films, the reflectivity values do not decrease considerably for the analyzed spectral range.

The reflectance spectra depend considerably on the fabrication-process parameters. In particular, the lowest reflectance values are obtained for sample T-1 and a minimum reflectance of 0.6% at 633 nm. Table 2 shows a comparison of reflection average of present work with similar type in bibliography; a good performance is evident.

The performance of an antireflective coating is measured for solar cells by [35]:

$$Rw = \frac{\int_{\lambda\ min}^{\lambda\ max} R(\lambda)\, N_{ph}(\lambda)\, d(\lambda)}{\int_{\lambda\ min}^{\lambda\ max} N_{ph}(\lambda)\, d(\lambda)} \quad (1)$$

where $R(\lambda)$ is the wavelength dependent reflection and $N_{ph}$ is the photon flux, AM1.5 spectrum, of the solar spectrum. *Rw* was calculated for two wavelength ranges for the sample T-1.

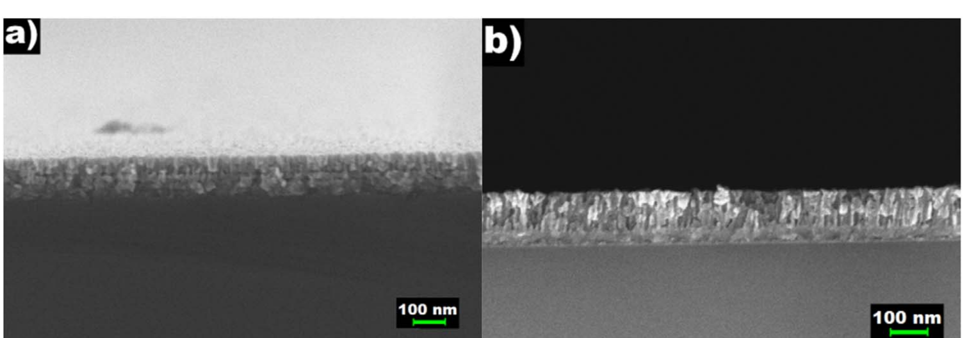


**Fig. 1.** Cross-sectional SEM images of the $TiO_2$ samples with different thickness (a) T-1 (b) M-1.

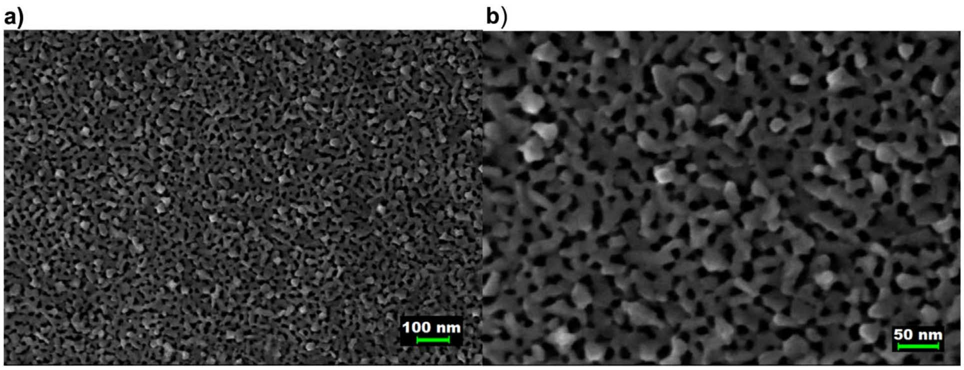


**Fig. 2.** Top-view SEM images of the $TiO_2$ sample M-1 (a) low and (b) high magnification.

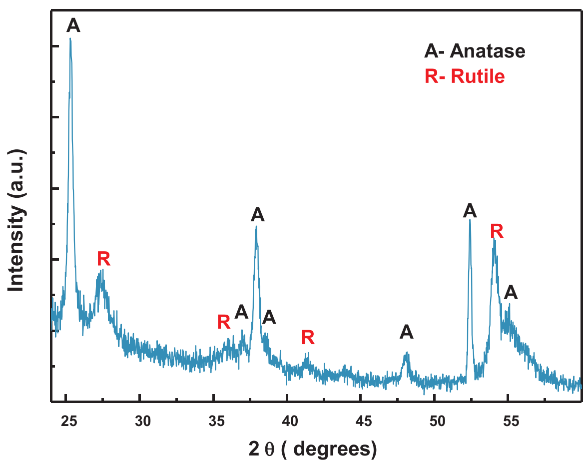


**Fig. 3.** X-ray diffraction pattern of the $TiO_2$ after annealed.

*Rw* (400–800 nm) = 0.02453 (o 2.4%)
*Rw* (200–900 nm) = 0.04244 (o 4.2%)

### 3.3. Ellipsometric models

The ellipsometric parameters $\psi(\lambda)$ and $\Delta(\lambda)$ were used to obtain the optical properties of the film using two model involving: Model 1: two layers and silicon substrate. The bottom and the top layers are dense and porous layers of $TiO_2$, respectively (Fig. 5).

The values of refractive index are obtained by Cauchy transparent model [36] described in Eq. (2).

$$n(\lambda) = A + \frac{10^4 B}{\lambda^2} + \frac{10^9 C}{\lambda^4} \tag{2}$$

where *A*, *B* and *C* are the model parameters.

The top layer is porous; it is formed by a mixture $TiO_2$ and void. The values of effective refractive index are obtained by the Bruggeman effective medium approximation [36].

Model 2: Several layers and the silicon substrate. A dense bottom layer of $TiO_2$ and the upper layers are porous; each one is formed by $TiO_2$ and vacuum in a composition gradient. Fig. 6 shows an schematic representation of the proposed physical model 2.

Model 1 was applied to adjust the optical data of the films. Fig. 7 shows the experimental and adjusted data of the spectroscopic ellipsometer for T-1 and M-1 as an example of each of the thicknesses.

Table 3 shows the adjusted results for these samples, the value of $\chi^2$ was also included as an indicator of the quality of fit. The fit was very suitable for the thinner samples and acceptable for the thicker ones. The values for thickness are directly compared with obtained from cross sectional SEM. It can be seen that the values are similar for both film thickness. Using the values of fitting parameters *A*, *B*, *C* and Eq. (1) were obtained the refractive indices of the dense layer. The refractive index of T-1 sample was similar with the values of the literature [37,38]. In contrast, the value of the M-1 sample was lower. This value is probably inadequate because the model 1 is very simple and it is necessary to consider a more complex model.

Model 2 was applied to adjust the optical data of the films using two layers as porous layer. Fig. 8 shows the experimental and adjusted data

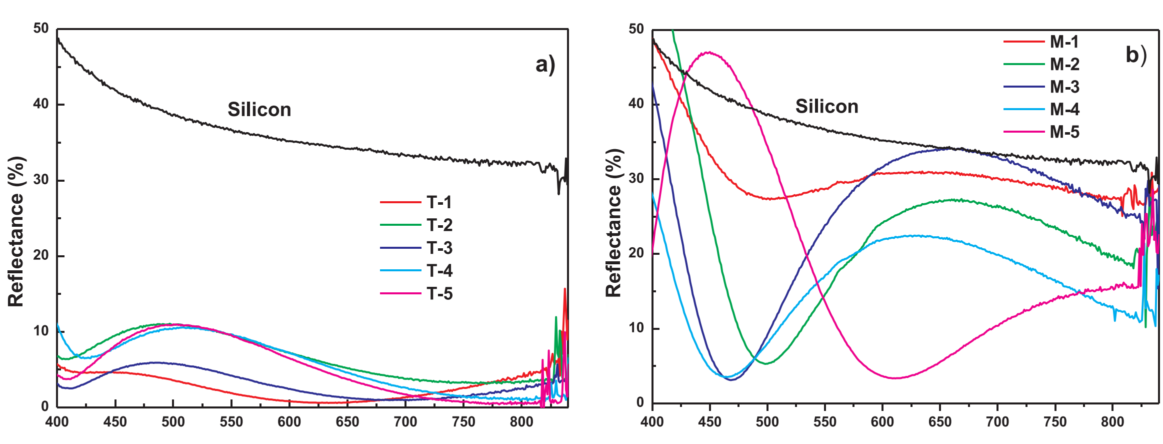


**Fig. 4.** Reflectance spectra of $TiO_2$ films on Si substrate as a function of wavelength with different thickness (a) T and (b) M.

**Table 2**
Comparison of antireflective coating of different materials on silicon substrate.

| No. | Reflection average (%) | Range (nm) | Materials | Layers | Ref. |
|---|---|---|---|---|---|
| 1 | 3.3 | 400–800 | $Al_2O_3/TiO_2$ | 2 | [26] |
| 2 | 6.2 | 400–1000 | $SiO_2/SiO_2$-$TiO_2/TiO_2$ | 3 | [27] |
| 3 | 14 | 400–1000 | NiO | 2 | [28] |
| 4 | 3.8 | 700 | Hydrogenated diamond like carbon | 1 | [29] |
| 5 | 6 | 300–1100 | Si random nanostructures and nanoparticles | 1 | [30] |
| 6 | 3 | 300–1100 | $InO_3$ nanocones | 1 | [31] |
| 7 | 4 | 300–1100 | $SiN_x/SiO_xN_y$ | > 3 | [32] |
| 8 | 7.8 | 400–1000 | $ZnO/Al_2O_3$ core-shell nanorods | > 3 | [33] |
| 9 | < 5 | 300–1100 | Si nanorod | 1 | [34] |
| 10 | 10.4 | 400–800 | $TiO_2$ | 1 | [35] |
| | 15 | 350–1150 | | 2 | |
| 11 | 2.5 | 400–800 | $TiO_2$ | 1 | This work |

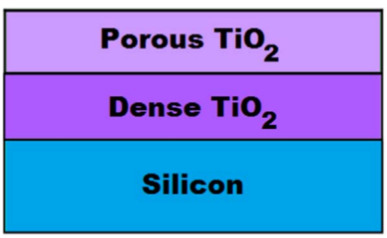


**Fig. 5.** Schematic representation of the proposed physical model 1.


**Fig. 6.** Schematic representation of the proposed physical model 2.

of the spectroscopic ellipsometer for the samples T-1 and M-1 to allow a comparison with model 1. Table 4 shows the adjusted results for these samples. The fit was very suitable for the thinner samples and acceptable for the thicker ones. The thicknesses are compared directly with the obtained values from cross sectional SEM.

The refractive indices of the films were calculated as a function of the wavelength using the adjustment values obtained with model 2. The refractive index of dense layer was about 2.3 for all samples. The calculated values of the refractive index of the top and bottom porous layer were approximately 1.6. The fact that the refractive index gradually decreases from the substrate to the air reduces the abrupt change in the silicon-air interface. Taking into account a specific multilayer model and the optical properties of each of the layers it is possible to optimize the optimum thicknesses to achieve the minimum reflectivity. This allows the layers of $TiO_2$ (dense) and $TiO_2$ (porous) to function as an antireflective coating.

It should be noted that by varying the anodizing parameters it is possible to adjust the optical properties within a certain range to achieve very low reflectivity values. At higher anodizing voltage, the greater inner diameter and the lower the percentage of $TiO_2$ in the porous layer achieving decrease the refractive index. Increasing anodization time it is possible to obtain greater thickness of the porous layer.

In summary, by modifying the fabrication parameters of the films (e.g. deposited titanium thickness, anodizing voltage and annealing temperature) it is possible to modify the optical properties to achieve a very low reflectivity. In the present work it was possible to obtain an average reflectivity of 2.5% (400–800 nm).

## 4. Conclusions

In this paper, $TiO_2$ nanotube layer coating on silicon was prepared by a simple electrochemical anodization method. The results obtained by fitting ellipsometry spectra in the 400–800 nm range, using a multilayer model consisting of a dense bottom of $TiO_2$ and the top layers are porous; they are formed by a mixture $TiO_2$ and void. The refractive indices of the top and bottom $TiO_2$ layers were approximately 2.3 and 1.6, respectively.

The thicknesses and optical properties were adjusted by controlling the manufacturing parameters to achieve a coating with very low reflectivity. The average reflectance of the coated sample was 2.5%. This manufacturing process can be used for different optoelectronic applications such as solar cells.

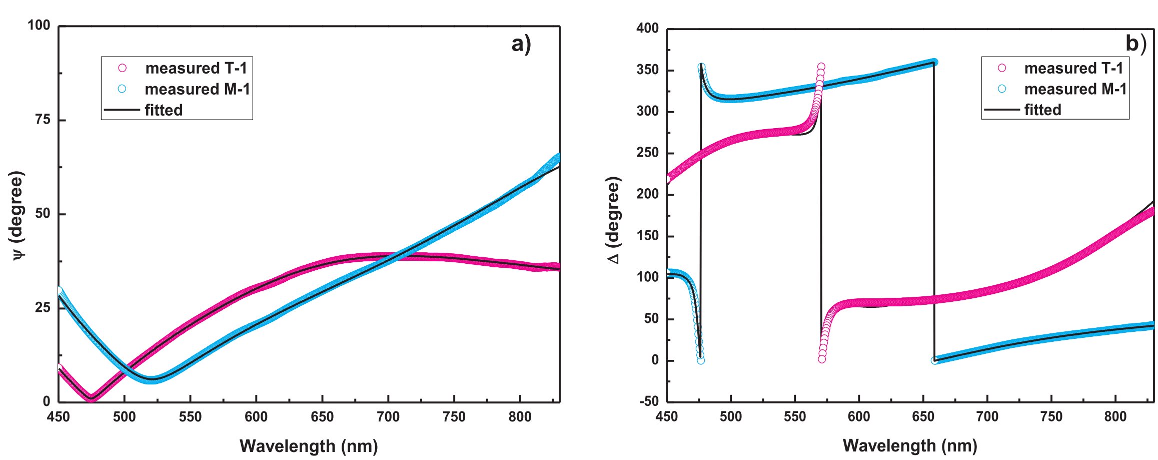


**Fig. 7.** Experimental data and fitted for T-1, M-1, using model 1 (a)$\psi$, (b) $\Delta$.

**Table 3**
Fitted results with proposed model 1.

| Sample | Thickness (nm) | | | | % TiO2 | Refractive index (at 600 nm) | | $\chi^2$ |
|---|---|---|---|---|---|---|---|---|
| | Dense layer | Porous layer | Total | Cross sectional SEM | Porous layer | Dense layer | Porous layer | |
| T-1 | 63 | 61 | 124 | 130 | 47 | 2.29 | 1.56 | 0.22 |
| M-1 | 74 | 116 | 190 | 170 | 61 | 1.84 | 1.46 | 1.36 |

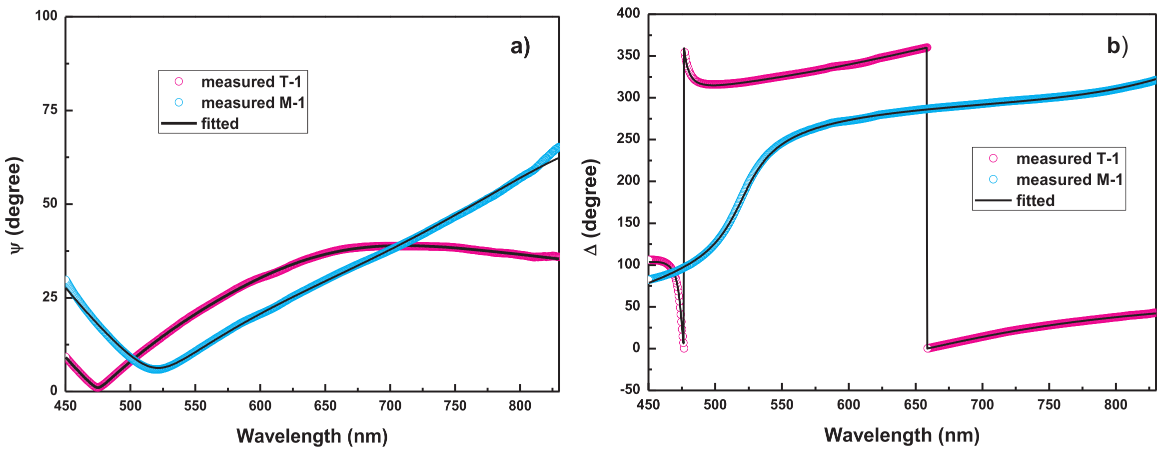


**Fig. 8.** Experimental data and fitted for T-1, M-1, using model 2 (a) $\psi$, (b) $\Delta$.

**Table 4**
Fitted results with proposed model 2.

| Sample | Thickness (nm) | | | | % TiO2 | | Refractive index (at 600 nm) | | | $\chi^2$ |
|---|---|---|---|---|---|---|---|---|---|---|
| | Dense layer | Porous layer | Total | Cross sectional SEM | Porous layer | | Dense layer | Porous layer | | |
| | | | | | Bottom | Top | | Bottom | Top | |
| T-1 | 60 | 64 | 124 | 130 | 50 | 44 | 2.31 | 1.57 | 1.55 | 0.23 |
| M-1 | 23 | 170 | 193 | 170 | 50 | 40 | 2.31 | 1.57 | 1.54 | 1.91 |

## Acknowledgments

The authors would like to acknowledge Daniel Vega from Condensed Matter Division, GAYANN, CNEA for XRD analysis.

## References

[1] X. Zhang, J. Zhang, Y. Jia, P. Xiao, J. Tang, $TiO_2$ nanotube array sensor for detecting the $SF_6$ decomposition product $SO_2$, Sensors 12 (2012) 3302–3313.
[2] G. Wu, J. Zhang, X. Wang, J. Liao, H. Xia, Sh.A. Akbar, J. Li, Sh. Lin, X. Li, J. Wang, Hierarchical structured $TiO_2$ nanotubes for formaldehyde sensing, Ceram. Int. 38 (2012) 6341–6347.
[3] P.M. Perillo, D.F. Rodríguez, N.G. Boggio, $TiO_2$ nanotubes for room temperature toluene sensor, OALIBj 1 (2014) 1–7.
[4] M. Barrera, J. Plá, C. Bocchi, A. Migliori, Antireflecting-passivating dielectric films on crystalline silicon solar cells for space applications, Sol. Energy Mater. Sol. Cells 92 (9) (2008) 1115–1122.
[5] J.-J. Liu, W.-J. Ho, Y.-Y. Lee, Ch.-M. Chang, Simulation and fabrication of $SiO_2$/graded-index $TiO_2$ antireflection coating for triple-junction GaAs solar cells by using the hybrid deposition process, Thin Solid Films 570 (2014) 585–590.
[6] V. Müller, P. Schmuki, Efficient photocatalysis on hierarchically structured $TiO_2$ nanotubes with mesoporous $TiO_2$ filling, Electrochem. Commun. 42 (2014) 21–25.
[7] Th.S. Natarajan, J.Y. Lee, H.C. Bajaj, W.-K. Jo, R.J. Tayade, Synthesis of multiwall carbon nanotubes/$TiO_2$ nanotube composites with enhanced photocatalytic decomposition efficiency, Catal. Today 282 (Part 1) (2017) 13–23.
[8] D.F. Rodríguez, P.M. Perillo, $TiO_2$ nanopores with high sensitivity to ultraviolet light, Opt. Mater. 42 (2015) 52–55.
[9] D.-Y. Zhang, C.-Wang Ge, J.-Zhen Wang, T.-Fei Zhang, Y.-Cheng Wu, F.-Xia Liang, Single-layer graphene-$TiO_2$ nanotubes array heterojunction for ultraviolet photodetector application, Appl. Surf. Sci. 387 (2016) 1162–1168.
[10] A. Lamberti, C.F. Pirri, $TiO_2$ nanotube array as biocompatible electrode in view of implantable supercapacitors, J. Energy Storage 8 (2016) 193–197.
[11] Sh.S. Raut, G.P. Patil, P.G. Chavan, B.R. Sankapa, Vertically aligned $TiO_2$ nanotubes: highly stable electrochemical supercapacitor, J. Electroanal. Chem. 780 (2016) 197–200.
[12] D.-S. Wuu, Ch.-Ch. Lin, Ch.-N. Chen, H.-H. Lee, J.-J. Huang, Properties of double-layer $Al_2O_3$/$TiO_2$ antireflection coatings by liquid phase deposition, Thin Solid Films 584 (2015) 248–252.
[13] A.T. Salih, A.A. Najim, M.A.H. Muhi, K.R. Gbashi, Single-material multilayer ZnS as anti-reflective coating for solar cell applications, Opt. Commun. 388 (2017) 84–89.
[14] L. Miao, L. Fen Su, S. Tanemura, C.A.J. Fisher, L.L. Zhao, Q. Liang, G. Xu, CosT − effective nanoporous $SiO_2$–$TiO_2$ coatings on glass substrates with antireflective and self-cleaning properties, Appl. Energy 112 (2013) 1198–1205.
[15] J.A. Dobrowolski, Optical properties of films and coatings, in: M. Bass (Ed.), Handbook of Optics, Chapter 42, Mc Graw-Hill, New York, USA, 1995.
[16] D.Z. Dimitrov, Chen-Hsun Du, Crystalline silicon solar cells with micro/nano texture, Appl. Surf. Sci. 266 (2013) 1–4.
[17] J.Q. Xi, M.F. Schubert, Jong Kyu Kim, E.F. Schubert, Minfeng Chen, Shawn-Yu Lin, W. Liu, J.A. Smart, Optical thin-film materials with low refractive index for broadband elimination of Fresnel reflection, Nat. Photonics 1 (2007) 176–179.
[18] Ch.-Ch. Chung, B.T. Tran, K.-L. Lin, T.-T. Ho, H.-W. Yu, N.-H. Quang, E.Y. Chang, Efficiency improvement of InGaP/GaAs/Ge solar cells by hydrothermal-deposited ZnO nanotube structure, Nanoscale Res. Lett. 9 (338) (2014) 1–5.
[19] D.F. Rodríguez, P.M. Perillo, Influence of fluoride content on the anodic formation of $TiO_2$ nanopores/nanotubes in Ti films, AASCIT Commun. 2 (1) (2015) 11–17.
[20] P.M. Perillo, D.F. Rodríguez, Growth control of $TiO_2$ nanotubes in different physical environments, Nanosci. Methods 1 (2012) 194–200.
[21] A. Jaroenworaluck, D. Regonini, C.R. Bowen, R. Stevens, A microscopy study of the effect of heat treatment on the structure and properties of anodised $TiO_2$ nanotubes, Appl. Surf. Sci. 256 (2010) 2672–2679.
[22] P. Schmuki, S.P. Albu, Influence of anodization parameters on the expansion factor of $TiO_2$ nanotubes, Electrochim. Acta 91 (2013) (90–55).
[23] D.J. LeClere, A. Velota, P. Skeldon, G.E. Thompson, S. Berger, J. Kunzeb, P. Schmuki, H. Habazakic, S. Nagata, Tracer investigation of pore formation in anodic titania, J. Electrochem. Soc. 155 (9) (2008) C487–C494.
[24] S. Bauer, H. Kleber, P. Schmuki, $TiO_2$ nanotubes: tailoring the geometry in $H_3PO_4$/HF electrolytes, Electrochem. Commun. 8 (8) (2006) 1321–1325.
[25] J.M. Macak, H. Hildebrand, U. Marten-Jahns, P. Schmuki, Mechanistic aspects and growth of large diameter self-organized $TiO_2$ nanotubes, J. Electroanal. Chem. 621

(2) (2008) 254–266.
[26] D.S. Wuu, C.C. Lin, C.N. Chen, H.H. Lee, J.J. Huang, Properties of double-layer $Al_2O_3/TiO_2$ antireflection coatings by liquid phase deposition, Thin Solid Films 584 (2015) 248–252.
[27] S.Y. Lien, D.S. Wuu, W.C. Yeh, J.C. Liu, Tri-layer antireflection coatings ($SiO_2$/$SiO_2$–$TiO_2$/$TiO_2$) for silicon solar cells using a sol–gel technique, Sol. Energy Mater. Sol. Cells 90 (2006) 2710–2719.
[28] M. Jlassi, I. Sta, M. Hajji, H. Ezzaouia, NiO thin films synthesized by sol-gel: potentiality for the realization of antireflection layer for silicon based solar cell applications, Surf. Interfaces 6 (2017) 218–222.
[29] D. Das, A. Banerjee, Anti-reflection coatings for silicon solar cells from hydrogenated diamond like carbon, Appl. Surf. Sci. 345 (2015) 204–215.
[30] L. Yang, Y. Xuan, Broadband and multi angle enhanced antireflection of silicon solar cells by compound random nanostructures, J. Quant. Spectrosc. Radiat. Transf. 151 (2015) 5–12.
[31] P. Prathap, et al., Anti-reflection — $In_2O_3$ nanocones for silicon solar cells, Sol. Energy 106 (2014) 102–108.
[32] J.D. Li, G.S. Shen, W.L. Chen, Z. Li, R.J. Hong, Preparation of $SiN_x$ multilayer films by mid-frequency magnetron sputtering for crystalline silicon solar cells, Mater. Sci. Semicond. Process. 59 (2017) 40–44.
[33] Ch.-M. Lung, W.-Ch. Wang, Ch.-H. Chen, L.-Y. Chen, M.-J. Chen, ZnO/Al2O3 core/shell nanorods array as excellent anti-reflection layers on silicon solar cells, Mater. Chem. Phys. 180 (2016) 195–202.
[34] D. Wang, Z. Yang, F. Li, D. Liu, P. Wang, D. He, Broadband antireflection of silicon nanorod arrays prepared by plasma enhanced chemical vapor deposition, Appl. Surf. Sci. 258 (3) (2011) 1058–1061.
[35] B.S. Richards, Single-material $TiO_2$ double-layer antireflection coatings, Sol. Energy Mater. Sol. Cells 79 (2003) 369–390.
[36] F.A. Jenkins, H.E. White, Fundamentals of Optics, 4th ed., McGraw-Hill, Inc., New York, 1981.
[37] D. Li, M. Carette, A. Granier, J.P. Landesman, A. Goullet, A. Spectroscopic ellipsometry analysis of TiO2 films deposited by plasma enhanced chemical vapor deposition in oxygen/titanium tetraisopropoxide plasma, Thin Solid Films 522 (2012) 366–371.
[38] D.F. Edwards, Titanium dioxide (TiO2) (Rutile), in: E. Palik (Ed.), Handbook of Optical Constants of Solids, Academic Press, San Diego, USA, 1985.